Non-Abelian operation on chiral Majorana fermions by quantum dots

Yan-Feng Zhou,[1,2] Zhe Hou,[1,2] and Qing-Feng Sun[1,2,3,*]

[1]*International Center for Quantum Materials, School of Physics, Peking University, Beijing 100871, China*

[2]*Collaborative Innovation Center of Quantum Matter, Beijing 100871, China*

[3]*CAS Center for Excellence in Topological Quantum Computation, University of Chinese Academy of Sciences, Beijing 100190, China*

(Received 24 December 2018; revised manuscript received 27 March 2019; published 22 May 2019)

We show that if a quantum dot or Majorana zero mode couples to the chiral Majorana fermions, a resonant exchange of chiral Majorana fermions can occur and leads to a non-Abelian braidinglike operation analogous to the braiding of Majorana zero modes. Remarkably, any operation in the braid group can be achieved by this scheme. We further propose electrical transport experiments to observe the braidinglike operation on four chiral Majorana fermions and demonstrate the non-Abelian character in four-terminal devices of the quantum anomalous Hall insulator/topological superconductor hybrid junctions. Both a conductance peak due to the operation and the operation-order-dependent conductance are predicted. These findings pave the way to perform any non-Abelian operation on chiral Majorana fermions by electrically controllable quantum dots.

DOI: 10.1103/PhysRevB.99.195137

I. INTRODUCTION

The Majorana fermion, which is its own antiparticle, was originally introduced as a putative elementary particle by Ettore Majorana and has been pursued as a quasiparticle excitation in condensed-matter systems [1–3]. Quantum information can be stored nonlocally in the degenerate ground-state space generated by the zero-energy Majorana excitations. Because of the non-Abelian braiding statistics [4,5], that information can be manipulated through the exchange of the Majorana excitations, which leads to a noncommutative transformation between different ground states. The final state is determined by the topology of the braiding and is robust against local perturbation, with possible applications in topological quantum computation [6–10].

For the zero-dimensional case, Majorana zero modes (MZMs) are predicted as midgap states bound to charge-$e/4$ quasiparticles of $\nu = 5/2$ fractional quantum Hall effect [4,11–13] and Abrikosov vortices in topological superconductors (TSCs) [5,14–16]. Moreover, alternative proposals suggest that a semiconducting nanowire coupled with a superconductor can also support MZMs localized at the wire ends [17–19], and mounting experimental progress in pursuing MZMs in these systems has been achieved by measuring the zero-bias peak of tunneling spectroscopy [20–23]. Despite the architectures proposed for performing the braiding operations of MZMs [10,24–27], the experimental realization remains an ongoing challenge.

As the one-dimensional analog of MZMs, chiral Majorana fermions emerge as unidirectionally propagating edge modes surrounding the edge of the $p + ip$ TSC [15,28–37]. The TSC has a full pairing gap classified by topological Chern number $\mathcal{N}$, which also determines the number of chiral Majorana edge modes. Theoretical proposals show that such an exotic superconductivity could arise by bringing certain topological matters in proximity to an s-wave superconductor [15,29]. By coupling an s-wave superconductor to a quantum anomalous Hall insulator (QAHI) realized in magnetic topological insulator thin films [38,39], a half-integer conductance plateau resulting from the chiral Majorana fermion was predicted [33,40], serving as a signature of a TSC with $\mathcal{N} = 1$. Unlike for the MZMs, few researchers have addressed the possible benefits of chiral Majorana fermions in the development of topological quantum computation [41,42]. In contrast to bounded MZMs, the chiral Majorana fermion is extended, providing a promising platform for scalable quantum computations.

In this paper, we propose a strategy to realize the non-Abelian braidinglike operation on chiral Majorana fermions coupled with a quantum dot (QD) or MZM. Let us first recall the electron resonance tunneling through the lead/QD/lead system [43,44]. Considering a system consisting of a QD coupled to two leads as shown in Fig. 1(a), an electron can resonantly tunnel from a lead through the QD to the other lead when the energy level of the QD is zero. However, when the energy level is far from zero, the electron tunneling is forbidden, and complete reflection occurs. Motivated by the electron resonant tunneling through a QD in the lead/QD/lead system, we show that if two chiral Majorana fermions $\gamma_{1,2}$ are coupled to a MZM, a resonant tunneling of Majorana fermions occurs and leads to a resonant exchange that sends $\gamma_1 \to -\gamma_2$ and $\gamma_2 \to -\gamma_1$ [see Fig. 1(b)]. On the other hand, a single chiral Majorana fermion coupled with a MZM acquires a negative sign. Our key idea is that by combining these two effects due to the coupling with MZMs [see Fig. 1(d)], γ_1 and γ_2 are transformed according to $\gamma_1 \to \gamma_2$ and $\gamma_2 \to -\gamma_1$, reminiscent of the braiding of MZMs. Then we demonstrate that such a braidinglike operation on chiral Majorana fermions could be completely reproduced by replacing MZMs with QDs, which are well constructed and can be controlled by the gate voltage in experiments [45–47]. We further propose a four-terminal

*sunqf@pku.edu.cn

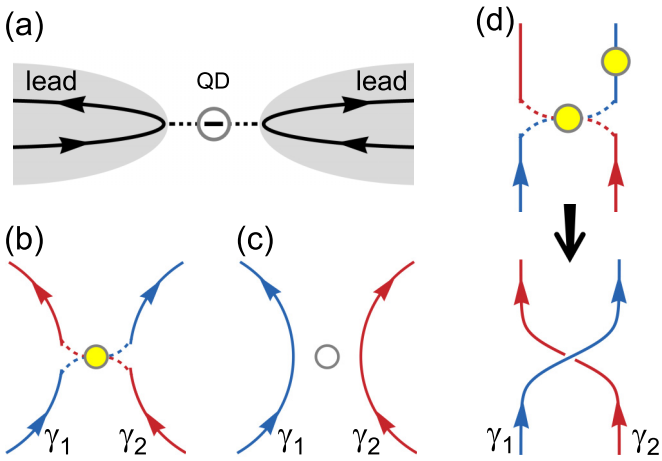

FIG. 1. (a) The resonant tunneling of an electron occurs in a lead/QD/lead model. (b) Two chiral Majorana fermions, γ_1 (blue arrow) and γ_2 (red arrow), are coupled to a MZM (yellow solid circle), and the coupling leads to a resonant exchange $\gamma_1 \to -\gamma_2$ and $\gamma_2 \to -\gamma_1$. (c) When the MZM is absent or disabled, as indicated by an open circle, γ_1 and γ_2 propagate independently. (d) The braidinglike operation on chiral Majorana fermions according to $\gamma_1 \to \gamma_2$ and $\gamma_2 \to -\gamma_1$ can be realized if one couples two MZMs to $\gamma_{1,2}$.

setup of the hybrid TSC/QAHI junction to observe the braidinglike operation on four chiral Majorana fermions indicated by a resonant conductance peak. Remarkably, our proposed system can be extended to carry out any operation in the braid group. For a sequential exchange process, the resonant conductance peak has a value of $\frac{e^2}{2h}$ or $\frac{e^2}{h}$ depending on the exchange order, which means the non-Abelian character of the operation.

The rest of the paper is organized as follows. After this introductory section, Sec. II provides the Hamiltonian describing two chiral Majorana fermions coupled to a MZM and the scattering matrix describing transmission between the chiral Majorana fermions. Then, in Sec. III, the Hamiltonian and scattering matrix in the QD coupling case are presented. In Sec. IV A, an experimental device for observing the braidinglike operation is proposed, and transport properties are studied. Then, a proposal for demonstrating the non-Abelian character of the operations is shown in Sec. IV B. Moreover, we show a universal device for executing various braidinglike operations controlled by gates in Sec. IV C. Section V concludes this paper. Some auxiliary materials are relegated to the Appendixes.

II. MAJORANA ZERO MODE COUPLING CASE

We begin by investigating the MZM coupling case in which a MZM is coupled to a pair of chiral Majorana fermions as shown in Fig. 1(b). The low-energy Hamiltonian of two decoupled chiral Majorana fermions is

$$H_0 = i\nu \sum_{\alpha=1,2} \int_{-\infty}^{+\infty} \gamma_\alpha(x)\partial_x\gamma_\alpha(x)dx, \tag{1}$$

where $\gamma_\alpha(x)$ is the field operator of chiral Majorana fermions, with $\gamma_\alpha^\dagger(x) = \gamma_\alpha(x)$ satisfying $\{\gamma_\alpha(x), \gamma_\beta(x')\} = \delta_{\alpha\beta}\delta_{xx'}$, and ν denotes the Fermi velocity. Let $H_{\rm M} = \sum_{\alpha=1,2} it_\alpha\gamma_\alpha(0)\gamma_0$ describe the coupling term between the MZM γ_0 ($\gamma_0^\dagger = \gamma_0$ and $\{\gamma_0, \gamma_0\} = 1$) and $\gamma_\alpha(x)$ at $x = 0$ with strength t_α. Then the total Hamiltonian is

$$H_1 = H_0 + H_{\rm M}. \tag{2}$$

When MZM γ_0 is absent, as denoted by an open circle in Fig. 1(c), γ_1 and γ_2 propagate independently, determined by H_0. If we switch on γ_0, as indicated by a yellow solid circle in Fig. 1(b), the scattering between γ_1 and γ_2 occurs at $x = 0$ due to the coupling with a MZM. In order to study the transport process, we first calculate the scattering matrix of the chiral Majorana fermions described by H_1 in Eq. (2).

By investigating the equations of motion for the field operators, i.e., $i\partial_t\gamma_i = [\gamma_i, H_1]$ ($i = 0, 1, 2$) in the Heisenberg picture, it can be found that the operators obey the differential equations of motion,

$$i\partial_t\gamma_\alpha(x,t) = 2i\nu\partial_x\gamma_\alpha(x,t) + it_\alpha\delta(x)\gamma_0(t), \tag{3}$$

$$i\partial_t\gamma_0(t) = -\sum_{\alpha=1,2} it_\alpha\gamma_\alpha(0,t). \tag{4}$$

Note that we have used the anticommutation relations to derive these equations. By the Fourier transformation of $\gamma_\alpha(x,t)$ and $\partial_t\gamma_\alpha(x,t)$,

$$\gamma_\alpha(x,\varepsilon) = \int_{-\infty}^{+\infty} \gamma_\alpha(x,t)e^{i\varepsilon t}dt, \tag{5}$$

$$\varepsilon\gamma_\alpha(x,\varepsilon) = \int_{-\infty}^{+\infty} [i\partial_t\gamma_\alpha(x,t)]e^{i\varepsilon t}dt, \tag{6}$$

the differential equations (3) and (4) become

$$\varepsilon\gamma_\alpha(x,\varepsilon) = 2i\nu\partial_x\gamma_\alpha(x,\varepsilon) + it_\alpha\delta(x)\gamma_0(\varepsilon), \tag{7}$$

$$\varepsilon\gamma_0(\varepsilon) = -\sum_{\alpha=1,2} it_\alpha\gamma_\alpha(0,\varepsilon). \tag{8}$$

Integrating both sides of Eq. (7) from 0^- to 0^+, we obtain

$$2i\nu[\gamma_\alpha(0^+) - \gamma_\alpha(0^-)] + it_\alpha\gamma_0 = 0. \tag{9}$$

Here, the variable ε has been left out for simplicity. Using Eq. (8) and $\gamma_\alpha(0) = \frac{\gamma_\alpha(0^+)+\gamma_\alpha(0^-)}{2}$, one arrives at

$$\left(2i\nu + \frac{t_1^2}{2\varepsilon}\right)\gamma_1(0^+) + \frac{t_1t_2}{2\varepsilon}\gamma_2(0^+) = \left(2i\nu - \frac{t_1^2}{2\varepsilon}\right)\gamma_1(0^-) - \frac{t_1t_2}{2\varepsilon}\gamma_2(0^-), \tag{10}$$

$$\frac{t_1t_2}{2\varepsilon}\gamma_1(0^+) + \left(2i\nu + \frac{t_2^2}{2\varepsilon}\right)\gamma_2(0^+) = -\frac{t_1t_2}{2\varepsilon}\gamma_1(0^-) + \left(2i\nu - \frac{t_2^2}{2\varepsilon}\right)\gamma_2(0^-). \tag{11}$$

Denoting the incoming and outgoing scattering states of the chiral Majorana fermions by $\gamma_{1/2}(0^-)$ and $\gamma_{1/2}(0^+)$,

respectively, the scattering matrix can be written as

$$\begin{pmatrix}\gamma_1(0^+)\\ \gamma_2(0^+)\end{pmatrix} = S_{\rm M}\begin{pmatrix}\gamma_1(0^-)\\ \gamma_2(0^-)\end{pmatrix}. \tag{12}$$

Solving Eqs. (10) and (11), we get the scattering matrix $S_{\rm M}$:

$$S_{\rm M} = \frac{1}{A}\begin{pmatrix}4i\varepsilon\nu + t_2^2 - t_1^2 & -2t_1t_2\\ -2t_1t_2 & 4i\varepsilon\nu + t_1^2 - t_2^2\end{pmatrix}, \tag{13}$$

in which $A = 4i\varepsilon\nu + t_1^2 + t_2^2$ and ε is the incident energy. The off-diagonal elements of the $S_{\rm M}$ matrix correspond to the amplitude for transmission between γ_1 and γ_2. The resulting transmission coefficient is $T(\varepsilon) = |S_{\rm M,12}|^2 = \frac{4\Gamma_1\Gamma_2}{4\varepsilon^2+(\Gamma_1+\Gamma_2)^2}$, with $\Gamma_\alpha \equiv t_\alpha^2/(2\nu)$, which is the same as the Breit-Winger formula describing the resonant scattering of the lead/QD/lead system.

Similar to the resonant tunneling process in the lead/QD/lead system [43,44] [see Fig. 1(a)], if the value of ε largely deviates from zero, the energy mismatch disables MZM γ_0, and no transmission happens with $T = 0$, as illustrated in Fig. 1(c). However, it is obvious from Eq. (13) that when $\varepsilon = 0$ and $t_1 = t_2 = t$, the scattering matrix becomes $S_{\rm M} = \left(\begin{smallmatrix}0 & -1\\ -1 & 0\end{smallmatrix}\right)$. In other words, when the energy of the incoming chiral Majorana fermions matches the energy of the MZM, there occurs a resonant exchange according to $\gamma_1 \to -\gamma_2$ and $\gamma_2 \to -\gamma_1$, as depicted in Fig. 1(b). Moreover, we consider the case that γ_0 is coupled only with γ_1 by setting $t_2 = 0$ and $t_1 = t$. Here, for $\varepsilon = 0$, the scattering matrix becomes $S_{\rm M} = \left(\begin{smallmatrix}-1 & 0\\ 0 & 1\end{smallmatrix}\right)$. This means that the phase of the chiral Majorana fermion can be changed by a value of π as $\gamma_1 \to -\gamma_1$, which can also be realized by the coupling with a metallic island [34,48]. More interestingly, it can be shown that two successive manipulations in which one MZM is first coupled simultaneously to γ_1 and γ_2 and then an additional one is coupled solely to γ_1 [see Fig. 1(d)] can produce a braidinglike operation on chiral Majorana fermions, $\gamma_1 \to \gamma_2$ and $\gamma_2 \to -\gamma_1$, like that in the braiding of MZMs. At this point, this result suggests that our method makes the non-Abelian operation on chiral Majorana fermions possible with the coupling of MZMs.

III. QUANTUM DOT COUPLING CASE

Considering that a zero-energy charged fermion bound state is topologically equivalent to a pair of MZMs [1], we want to know whether a QD with a single energy level can provide an alternative approach to transform the chiral Majorana fermions as well as a MZM. Next, we consider two chiral Majorana fermions coupled to a QD as shown in Fig. 2(a). The total Hamiltonian now becomes

$$H_2 = H_0 + H_{\rm QD} + H_{\rm C}, \tag{14}$$

where $H_{\rm QD} = \varepsilon_d d^\dagger d$ and $H_{\rm C} = \sum_{\alpha=1,2} i(\tilde{t}_\alpha/\sqrt{2})\gamma_\alpha(0)(d + d^\dagger)$ [49]. The second term, $H_{\rm QD}$, is the Hamiltonian of the QD with a single energy level ε_d, and $d^\dagger$ (d) are the creation (annihilation) operators of the fermion state in the QD. The third term, $H_{\rm C}$, describes the coupling between γ_α and the QD with coupling strength $\tilde{t}_\alpha$.

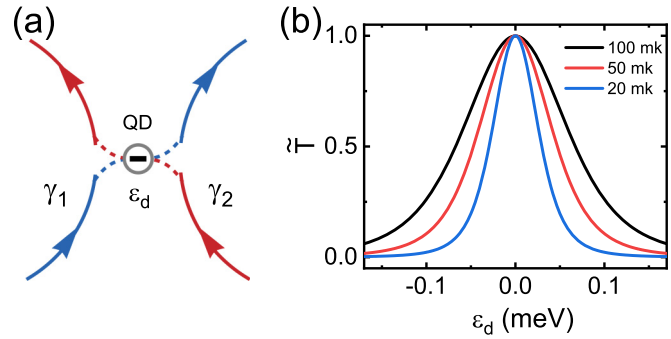

FIG. 2. (a) The chiral Majorana fermions γ_1 (blue arrow) and γ_2 (red arrow) are coupled to a QD with a single energy level ε_d. (b) The transmission $\widetilde{T}$ describing the scattering between γ_1 and γ_2 due to the QD coupling as a function of ε_d at different temperatures.

Similar to the MZM coupling case, the scattering matrix denoted by $S_{\rm Q}$ in this case can be derived as (see Appendix A for details)

$$S_{\rm Q} = \frac{1}{\widetilde{A}}\begin{pmatrix}\widetilde{B} + \tilde{t}_2^2 - \tilde{t}_1^2 & -2\tilde{t}_1\tilde{t}_2\\ -2\tilde{t}_1\tilde{t}_2 & \widetilde{B} + \tilde{t}_1^2 - \tilde{t}_2^2\end{pmatrix}, \tag{15}$$

where $\widetilde{B} = 4i\nu(\varepsilon^2 - \varepsilon_d^2)/\varepsilon$ and $\widetilde{A} = \widetilde{B} + \tilde{t}_1^2 + \tilde{t}_2^2$. For comparison with the MZM setting $\varepsilon_d = 0$, it can be found that the scattering matrix $S_{\rm Q}$ is the same as $S_{\rm M}$ in Eq. (13). To make this point more clearly, we define two Majorana operators, $\gamma_{d1} = (d + d^\dagger)/\sqrt{2}$ and $\gamma_{d2} = -i(d - d^\dagger)/\sqrt{2}$. Written in this Majorana basis, the coupling part in Eq. (14) becomes $H_C = \sum_{\alpha=1,2} i\tilde{t}_\alpha\gamma_\alpha(0)\gamma_{d1}$, which recovers H_M in the MZM coupling case, and the chiral Majorana edge modes decouple from one of the Majorana modes inside the QD. For the energy level $\epsilon_d = 0$, the Hamiltonian in Eq. (14) is the same as the Hamiltonian in Eq. (2). Therefore, the QD should be able to accomplish the braidinglike operation on chiral Majorana fermions like the MZM. On the other hand, in real experiments the energy level ε_d inside the QD can be tuned easily by gate voltages [45–47]. For finite ε_d, the transmission coefficient now becomes $\widetilde{T}(\varepsilon) = |S_{\rm Q,12}|^2 = \frac{4\widetilde{\Gamma}_1\widetilde{\Gamma}_2\varepsilon^2}{4(\varepsilon^2-\varepsilon_d^2)^2+(\widetilde{\Gamma}_1+\widetilde{\Gamma}_2)^2\varepsilon^2}$, with $\widetilde{\Gamma}_\alpha \equiv \tilde{t}_\alpha^2/(2\nu)$. Considering the nonzero temperature $\mathcal{T}$, the effective transmission coefficient is $\widetilde{\mathcal{T}} = \int_{-\infty}^{+\infty}\widetilde{T}(\varepsilon)(-\frac{\partial f}{\partial\varepsilon})d\varepsilon$, where $f(\varepsilon) = [\exp(\varepsilon/k_B\mathcal{T}) + 1]^{-1}$ is the Fermi distribution function. Figure 2(b) shows $\widetilde{\mathcal{T}}$ as a function of ε_d with $\widetilde{\Gamma}_1 = \widetilde{\Gamma}_2 \equiv \Gamma = 1$ meV at different temperatures. It can be seen that the transmission curves $\widetilde{\mathcal{T}}$ show obviously resonant behaviors with a peak at $\varepsilon_d = 0$ where the resonant exchange of chiral Majorana fermions occurs. If the value of ε_d deviates from zero, $\widetilde{\mathcal{T}}$ decreases with a full width at half maximum estimated to be $\sqrt{\Gamma k_B\mathcal{T}}$. When ε_d is far from zero, $\widetilde{\mathcal{T}}$ tends to zero, and the chiral Majorana fermions propagate independently without exchange, as shown in Fig. 1(c). This result implies an electrical method to control the braidinglike operation. In contrast to MZMs, the QDs are well constructed experimentally [47], and thus, the QDs are considered in the following discussion.

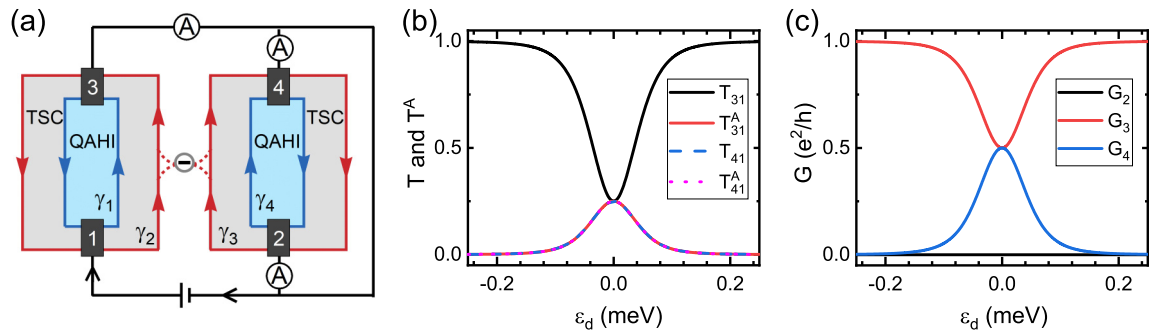

FIG. 3. (a) An experimental device based on TSC/QAHI junctions allows us to observe the braidinglike operation on four chiral Majorana fermions γ_i ($i = 1, 2, 3, 4$). The chirality of γ_i in the left part is different from the one in the right part as a result of the opposite magnetizations in the two regions. The QD can trigger the exchange of γ_2 and γ_3. (b) and (c) Transport coefficients for the transmission process for lead 1 to leads 3 and 4 and terminal conductance as a function of ε_d.

IV. EXPERIMENTAL PROPOSAL

A. Observation of the braidinglike operation

To observe the braidinglike operation on chiral Majorana fermions experimentally, we propose the electrical transport in a four-terminal device where two ribbons of hybrid TSC/QAHI junctions with opposite out-of-plane magnetizations are coupled by a QD, as depicted in Fig. 3(a). The QAHI was realized in magnetically doped topological insulators with Chern number $\mathcal{C} = 1$ and has one chiral Dirac edge mode around its boundary [38,39]. The theoretically proposed TSC by bring QAHI in proximity to an s-wave superconductor has a Chern number $\mathcal{N} = 1$, which corresponds to one chiral Majorana edge mode [15,29]. In view of the fact that there exists one chiral Majorana edge mode at the boundary between TSC and QAHI [33], the transport process in the device occurs via four chiral Majorana edge states γ_i ($i = 1, 2, 3, 4$), as denoted by red and blue arrows in Fig. 3(a). The QD between the TSC regions behaves as a switch for controlling the braidinglike operation on γ_2 and γ_3 and determines the terminal conductance. Considering that the chiral Majorana edge modes are localized at the edges with a localization length l_w [50], the width of the TSC and QAHI regions in Fig. 3(a) should be greater than the localization length to avoid hybridization between the Majorana edge modes. For an estimation, $l_w \sim v_F/\Delta = 0.52\ \mu$m, with the Fermi velocity of edge modes in QAHI $v_F \sim 2.6$ eV Å and the induced superconducting gap $\Delta \sim 0.5$ meV [33]. But the interval between the left and right hybrid TSC/QAHI ribbons [i.e., the interval between γ_2 and γ_3; see Fig. 3(a)] can be close to or less than l_w because the wave function of the Majorana edge state is zero outside the TSC and QAHI [50]. In real experiments, considering a QD with a size of 0.5 μm, the interval between the left and right TSC/QAHI ribbons can be set to 1 μm, and the QD can be placed in the middle of two TSCs in the center, as shown in Fig. 3(a).

The measured current in lead n can be calculated using the multiprobe Landauer-Büttiker formula [51–53]

$$I_n = \frac{e^2}{h}\sum_m T_{nm}(V_n - V_m) + T^A_{nm}(V_n + V_m), \tag{16}$$

where T_{nm} (T^A_{nm}) is the normal tunneling (Andreev reflection) coefficient from lead m to lead n and V_n is the voltage of terminal n. The voltage of lead 1 is fixed to V, and the voltages of leads 2, 3, and 4 have the same value U [see Fig. 3(a)]. These transport coefficients can be calculated from the scattering matrix S_Q in Eq. (15) (see Sec. B 1). With these coefficients, the currents of the leads become

$$I_1 = \frac{e^2}{h}T_{13}(V - U), \tag{17}$$

$$I_2 = 0, \tag{18}$$

$$I_3 = \frac{e^2}{h}\left[T_{31}(U - V) + T^A_{31}(U + V) + 2T^A_{32}U\right], \tag{19}$$

$$I_4 = \frac{e^2}{h}\left[T_{41}(U - V) + T^A_{41}(U + V) + 2T^A_{42}U\right]. \tag{20}$$

Then by the current conservation $I_1 + I_2 + I_3 + I_4 = 0$, one gets

$$U = \frac{T_{31} - T^A_{31} + T_{41} - T^A_{41} - T_{13}}{T_{31} + T^A_{31} + 2T^A_{32} + T_{41} + T^A_{41} + 2T^A_{42} - T_{13}}V. \tag{21}$$

The conductance of lead n is defined as $G_n = \frac{-I_n}{V_1 - V_n} = \frac{-I_n}{V - U}$, which can be obtained from Eqs. (17)–(21) straightforwardly.

Figures 3(b) and 3(c) display the transport coefficients and terminal conductance as functions of ε_d, respectively. If ε_d is tuned away from zero, the electrical transports in two ribbons are independent despite the QD ($T_{41} = T^A_{41} = 0$), and the normal tunneling process dominates with $T_{31} = 1$, leading to $G_3 = e^2/h$ and $G_4 = 0$. As ε_d approaches zero, the transmission between γ_2 and γ_3 takes place with a resonant exchange $\gamma_2 \to -\gamma_3$ and $\gamma_3 \to -\gamma_2$. As a result, the normal tunneling coefficient and Andreev reflection coefficient from lead 1 to both leads 3 and 4 are equal, i.e., $T_{31} = T^A_{31} = T_{41} = T^A_{41} = 1/4$, as shown in Fig. 3(b). Moreover, it can be seen from Fig. 3(c) that the conductance G_4 shows a peak of $\frac{e^2}{2h}$, while G_3 has a valley of $\frac{e^2}{2h}$, with $G_2 + G_3 + G_4 = \frac{e^2}{h}$ and $G_2 = 0$. If another QD is brought to couple with γ_2 after the resonant exchange, γ_2 acquires an additional sign change, and the braidinglike operation is carried out as $\gamma_2 \to \gamma_3$ and $\gamma_3 \to -\gamma_2$. However, the transmission coefficients from lead 1 to leads 3 and 4 are unaffected, and so is the conductance.

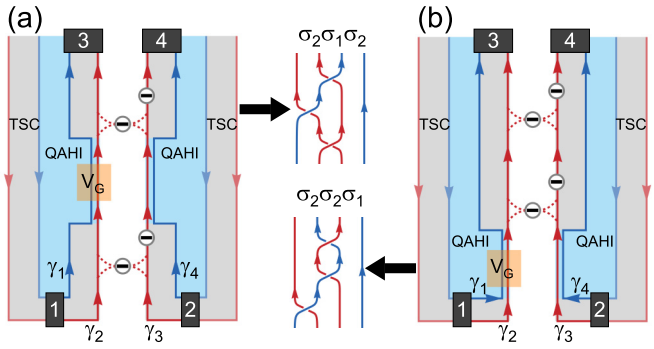

FIG. 4. Experimental devices providing a demonstration of the non-Abelian character. (a) and (b) Devices execute two joint operations constituted by three sequential braidinglike operations, $\sigma_2\sigma_1\sigma_2$ and $\sigma_2\sigma_2\sigma_1$, respectively. The different orders in the two operations yield completely different braidings of γ_i ($i = 1, 2, 3, 4$), as shown in the middle. The gate voltage V_G performs operator σ_1, and operator σ_2 is carried out by two successive QDs, as discussed in Fig. 1(d).

Therefore, such a conductance peak (valley) can provide an experimental signature for the braidinglike operations.

B. Demonstration of the non-Abelian character

In principle, there are infinite braidinglike operations on four chiral Majorana fermions forming a braid group similar to the braiding of MZMs. Any braiding operation in the group can be represented algebraically in terms of generators σ_i, with $i = 1, 2, 3$ [9]. The braidinglike operation of γ_α at the ith position and γ_β at the $(i+1)$th position can be formulated as a non-Abelian unitary transformation with the form $\sigma_i = e^{(\pi/2)\gamma_\beta\gamma_\alpha}$, where we retain i only in subscript for simplicity. Through a Taylor expansion, the expression becomes $\sigma_i = e^{(\pi/2)\gamma_{i+1}\gamma_i} = \frac{1}{\sqrt{2}}(1 + 2\gamma_\beta\gamma_\alpha)$. By performing the operation on $\gamma_{\alpha,\beta}$ and using the anticommutation relations, one obtains $\sigma_i\gamma_\alpha\sigma_i^{-1} = \gamma_\beta$ and $\sigma_i\gamma_\beta\sigma_i^{-1} = -\gamma_\alpha$ as the braidinglike operations. Now, we take the device with two ribbons of TSC/QAHI junctions in Fig. 4(a) as an example to show our strategy to execute all three generators. There are four chiral Majorana edge modes denoted by arrowed lines starting from leads 1 and 2. Similar to the discussion of Fig. 1(d), with the coupling of two successive QDs, the consequent operation completes σ_2, which braids the chiral Majorana fermions propagating along the central two red lines. Moreover, the gate voltage V_G of the left ribbon in Fig. 4(a) can induce an additional phase for the chiral QAHI edge state, leading to a transformation between the chiral Majorana fermions on the first and second lines sorted from left to right, which is equivalent to the braidinglike operation by σ_1 [41]. Similarly, the braidinglike operation by σ_3 can be carried out by placing a gate voltage on the QAHI edge of the right ribbon, as shown in Fig. 5. Accordingly, in view of the scalability of chiral Majorana edge modes, the proposed device provides a scalable platform to perform any braidinglike operation by an arbitrary combination of the three generators which can be controlled and tuned by the electrical method, and we clarify this point in the next section. Moreover, the proposed braidinglike operation on chiral Majorana fermions runs at the speed of the electric field, which is much faster than those of the MZM limited by the velocity of a moving domain wall in one-dimensional topological superconductors [54,55].

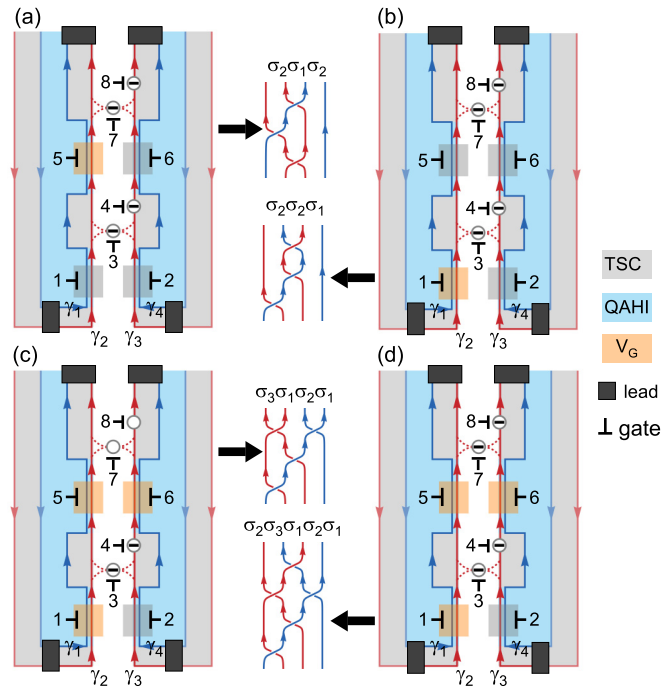

FIG. 5. Four representative operations realized in a universal device by tuning the gates. (a) By tuning gates 1, 2, and 6 away from the working conditions as represented by dark gray shaded regions, the resulting operation recovers $\sigma_2\sigma_1\sigma_2$ in Fig. 4(a). (b) The operation $\sigma_2\sigma_2\sigma_1$ by tuning gates 2, 5, and 6, reminiscent of Fig. 4(b). (c) and (d) Operations $\sigma_3\sigma_1\sigma_2\sigma_1$ and $\sigma_2\sigma_3\sigma_1\sigma_2\sigma_1$. The open circles in (c) mean that the energy level ε_d is tuned away from zero by gates 7 and 8 and the QDs cannot braid the chiral Majorana edge modes anymore. The middle shows the corresponding braidinglike operation on γ_i ($i = 1, 2, 3, 4$).

With this exciting possibility to carry out any braidinglike operation, we next propose the electrical transport experiments in the devices, as shown in Fig. 4, to observe the non-Abelian character where the sequential exchanges are executed in different orders. Here, we set $\varepsilon_d = 0$ for all the QDs. Let us define occupation number 0 or 1 of the QAHI edge states in the left and right ribbons as two qubits L and R with bases $|0_x\rangle$ and $|1_x\rangle$ ($x = L, R$) [41]. The degenerate ground-state space of the two qubits is expanded by four states, $|0_L0_R\rangle$, $|1_L0_R\rangle$, $|0_L1_R\rangle$, and $|1_L1_R\rangle$. In this basis, the generator σ_i which exchanges γ_i and γ_{i+1} is represented by a 4×4 unitary matrix $\rho(\sigma_i)$ acting on the states in the ground-state space as [5]

$$\rho(\sigma_1) = \begin{pmatrix} e^{-i\pi/4} & 0 & 0 & 0 \\ 0 & e^{+i\pi/4} & 0 & 0 \\ 0 & 0 & e^{-i\pi/4} & 0 \\ 0 & 0 & 0 & e^{+i\pi/4} \end{pmatrix}, \quad (22)$$

$$\rho(\sigma_2) = \frac{1}{\sqrt{2}} \begin{pmatrix} 1 & 0 & 0 & -i \\ 0 & 1 & -i & 0 \\ 0 & -i & 1 & 0 \\ -i & 0 & 0 & 1 \end{pmatrix}, \quad (23)$$

$$\rho(\sigma_3) = \begin{pmatrix} e^{-i\pi/4} & 0 & 0 & 0 \\ 0 & e^{-i\pi/4} & 0 & 0 \\ 0 & 0 & e^{+i\pi/4} & 0 \\ 0 & 0 & 0 & e^{+i\pi/4} \end{pmatrix}. \quad (24)$$

First, we consider two joint operators, $\sigma_2\sigma_1$ and $\sigma_1\sigma_2$. After the braidinglike operations, the chiral Majorana fermions $(\gamma_1, \gamma_2, \gamma_3, \gamma_4)$ are transformed to $(-\gamma_2, -\gamma_3, \gamma_1, \gamma_4)$ by $\sigma_2\sigma_1$ and to $(\gamma_3, \gamma_1, \gamma_2, \gamma_4)$ by $\sigma_1\sigma_2$, respectively. If we prepare the system in an initial state $|\psi_i\rangle = |1_L 0_R\rangle$ by injecting the electrons into qubit L one by one from lead 1 with weak current, it can be found that $\sigma_2\sigma_1$ turns the system into the final state $|\psi_{f1}\rangle = (|1_L 0_R\rangle - i|0_L 1_R\rangle)/\sqrt{2}$ and $\sigma_1\sigma_2$ turns it into a different state, $|\psi_{f2}\rangle = (|1_L 0_R\rangle - |0_L 1_R\rangle)/\sqrt{2}$, via the unitary matrices in Eqs. (22)–(24). Unfortunately, the two different final states cannot be distinguished by the proposed four-terminal device, in which we find $G_3 = G_4 = \frac{e^2}{2h}$ for both cases (see Sec. B2). Although the two joint operators are carried out in different orders, they both transport γ_1 and γ_2 coming from lead 1 to different leads (lead 3 and lead 4), and this leads to the same result for conductance measurements.

However, the operators constituted by three sequential exchanges, $\sigma_2\sigma_1\sigma_2$ and $\sigma_2\sigma_2\sigma_1$ in Fig. 4, yield very different results, indicating the non-Abelian character. In this situation, $(\gamma_1, \gamma_2, \gamma_3, \gamma_4)$ are transformed to $(\gamma_3, -\gamma_2, \gamma_1, \gamma_4)$ by $\sigma_2\sigma_1\sigma_2$ and to $(-\gamma_2, -\gamma_1, -\gamma_3, \gamma_4)$ by $\sigma_2\sigma_2\sigma_1$, as shown in the middle part of Fig. 4. From the initial state $|\psi_i\rangle = |1_L 0_R\rangle$, the device in Fig. 4(a) arrives at the final state $|\psi_{f2}\rangle = (|1_L 0_R\rangle - |0_L 1_R\rangle)/\sqrt{2}$ transformed by $\sigma_2\sigma_1\sigma_2$, while the joint operator $\sigma_2\sigma_2\sigma_1$ drives the device in Fig. 4(b) into final state $|\psi_{f3}\rangle = |0_L 1_R\rangle$ via the unitary matrices in Eqs. (22)–(24). As a result, the conductances observed in Fig. 4(a) are $G_3 = G_4 = \frac{e^2}{2h}$, but the ones in Fig. 4(b) are $G_4 = \frac{e^2}{h}$ and $G_3 = 0$ (see Sec. B 2). In the case of $\sigma_2\sigma_2\sigma_1$, γ_1 and γ_2 enter lead 3 together and recombine as a hole providing a different conductance measurement. These results provide a signature supporting the non-Abelian character of the braidinglike operations on chiral Majorana fermions.

In a real experiment, there may exist various decoherences, which possibly corrects the predicted conductance [41]. In our proposed experimental devices, two main mechanisms may lead to the decoherence. The first one is the nonmonochromaticity of the incident chiral Majorana edge states from the lead due to the thermal smearing. The thermal smearing may lead to a momentum uncertainty in the incident states from the lead $\triangle p \approx k_B\mathcal{T}/v$. As long as the two incident chiral Majorana edge states from lead 1 enter the same lead together, e.g., lead 3 or lead 4, they can recombine as an electron or a hole depending on their phase relation after the operations (zero or π) [34,50]. To keep the phase relation unchanged, the momentum uncertainty sets a length scale $\triangle L < \hbar/\triangle p$, where $\triangle L$ is the length scale for the path-length difference of the chiral Majorana edge states. For an estimation, the Fermi velocity [33] $\hbar v \sim 2.0$ eV Å, and the temperature $\mathcal{T} \sim 20$ mK; this sets an upper bound on the path-length difference $\triangle L \sim 100$ μm, which is feasible in real mesoscopic experiments. The second source of decoherence is the inelastic scattering process. The inelastic scatterers set up a length scale, i.e., the Thouless phase coherence length l_ϕ [56], on which the quantum coherence is maintained. In the quantum Hall states of a two-dimensional electron gas, the inelastic phonon scattering can be dramatically suppressed by a large magnetic field, and l_ϕ can exceed 100 μm at $\mathcal{T} \sim 20$ mK [57,58]. Due to the existence of chiral edge states in both QAHI and integer quantum Hall, the phase coherence length l_ϕ in the QAHI is expected to be comparable to that in integer quantum Hall. Furthermore, the phonon scattering on chiral Majorana fermions is negligible due to their charge neutrality, and the inelastic scattering of the interaction between chiral Majorana fermions will be suppressed to a great extent at low temperature [59]. As a result, the chiral Majorana edge modes in TSC should have a longer phase coherence length l_ϕ than the edge modes in QAHIs. Based on these estimates, l_ϕ can be over 100 μm at low temperature (e.g., $\mathcal{T} \sim 20$ mK). In combination with the above two points, the proposed non-Abelian operation should be feasible, and the predicted conductance should remain when the length of the hybrid TSC/QAHI junction ribbon is not more than 100 μm.

C. Universal device for executing various operations

In this section, we further propose a universal device for executing various braidinglike operations controlled by gates, as illustrated in Fig. 5 to show the advantages of our strategy. Similar to the devices in Fig. 4, the device shown in Fig. 5 is made of two ribbons of hybrid TSC/QAHI junctions with opposite out-of-plane magnetizations. Here, we introduce four QAHI regions covered by gate voltage V_G, as denoted by orange shaded regions, to carry out the braidinglike operator σ_1 (σ_3) controlled by gates 1 and 5 (2 and 6). Moreover, four QDs controlled by gates 3, 4, 7, and 8 are placed between the TSC regions to carry out the braidinglike operator σ_2. If all the operators controlled by the gates are working, the resulting operation is $\sigma_2\sigma_3\sigma_1\sigma_2\sigma_3\sigma_1$ and transforms $(\gamma_1, \gamma_2, \gamma_3, \gamma_4)$ into $(-\gamma_4, \gamma_3, -\gamma_2, \gamma_1)$. The advantage of our proposed device is that all the modules to realize the braiding operators are electrically controllable, and this point makes various operations available in a single device by tuning the gates.

In principle, there are 64 (2^6) combinations of σ_i ($i = 1, 2, 3$) which can be executed by the device in Fig. 5. Here, we show four representative operations. If one tunes gates 1, 2, and 6 away from the working conditions for operators σ_1 and σ_3, then the resulting operation is $\sigma_2\sigma_1\sigma_2$, as shown in Fig. 5(a), i.e., the joint operation in Fig. 4(a). Similarly, the joint operation $\sigma_2\sigma_2\sigma_1$ in Fig. 4(b) can be carried out by tuning gates 2, 5, and 6 away from the working conditions, as shown in Fig. 5(b). Moreover, if the energy level ε_d of the QDs deviates from zero, the braiding of chiral Majorana fermions is unrealizable, as indicated by open circle in Fig. 5(c). In Fig. 5(c), we disable the QDs controlled by gates 7 and 8 and V_G controlled by gate 2; then the consequent operation $\sigma_3\sigma_1\sigma_2\sigma_1$ transforms $(\gamma_1, \gamma_2, \gamma_3, \gamma_4)$ into $(\gamma_3, -\gamma_2, -\gamma_4, \gamma_1)$. If we switch on the QD again, as shown in Fig. 5(d), another operation, $\sigma_2\sigma_3\sigma_1\sigma_2\sigma_1$, is achieved, and $(\gamma_1, \gamma_2, \gamma_3, \gamma_4)$ are transformed to $(\gamma_3, \gamma_4, -\gamma_2, \gamma_1)$. The remaining operations can also be achieved by tuning the corresponding gates. In principle, such a universal device can be extended to include more complicated operations in view of the scalability of

chiral Majorana edge modes. However, in real experiments, the entanglements with surroundings and various imperfections may set bounds on the size of the devices, e.g., the phase coherence length discussed above. If the length of a hybrid TSC/QAHI junction ribbon is $L \sim 100$ μm and the size of each gate voltage and QD is 0.5 μm on average, there should be more than 100 operations. Actually, for all possible operations in the braiding group, the corresponding transformations on the Majorana fermions $(\gamma_1, \gamma_2, \gamma_3, \gamma_4)$ can lead only to permutations of their positions and a phase change (zero or π). Correspondingly, only a few states are available for the two qubits after the braidinglike operations, such as $(|1_L 0_R\rangle \pm |0_L 1_R\rangle)/\sqrt{2}$, $(|1_L 0_R\rangle \pm i|0_L 1_R\rangle)/\sqrt{2}$, $|0_L 1_R\rangle$, $|1_L 0_R\rangle$ up to a phase, from an initial state $|\psi_i\rangle = |1_L 0_R\rangle$. All these states can be obtained in the proposed universal device to execute various operations by tuning the gates.

V. CONCLUSION

To conclude, we proposed a method to perform a braidinglike operation on chiral Majorana fermions coupled with quantum dots or Majorana zero modes. A resonant exchange between a pair of chiral Majorana fermions coupled through a quantum dot or Majorana zero mode leads to the transformation $\gamma_1 \to -\gamma_2$ and $\gamma_2 \to -\gamma_1$. Subsequently, γ_1 acquires an additional sign change by a sole coupling with a quantum dot or Majorana zero mode. As a consequence, the resulting operation with $\gamma_1 \to \gamma_2$ and $\gamma_2 \to -\gamma_1$ recovers the braiding of Majorana zero modes. Moreover, transport experiments were proposed to observe such a braidinglike operation on chiral Majorana fermions in the hybrid topological superconductor/quantum anomalous Hall insulator junctions, and a signature of the conductance peak was predicted. Meanwhile, the non-Abelian character of the braidinglike operation would be demonstrated by an order-dependent conductance in the transport experiments. Especially, we proposed a universal device to carry out various braidinglike operations controlled by gates. This braidinglike scheme not only can provide a convincing signature of chiral Majorana fermions but can also pave a feasible way towards robust quantum computation.

ACKNOWLEDGMENTS

This work was financially supported by the National Key R and D Program of China (Grant No. 2017YFA0303301), NBRP of China (Grant No. 2015CB921102), NSF China (Grant No. 11574007), the Strategic Priority Research Program of the Chinese Academy of Sciences (Grant No. XDB28000000), and Beijing Municipal Science & Technology Commission No. Z181100004218001.

APPPENDIX A: SCATTERING MATRIX FOR THE QD COUPLING CASE

Similar to the procedure in the MZM coupling case, the equation of motion for the field operators is $i\partial_t O(t) = [O(t), H_2]$, where $O(t)$ stands for the field operators of chiral Majorana fermions and the fermion state inside the QD in Heisenberg picture and H_2 is defined in Eq. (14). Here, the differential equations for the operators become

$$i\partial_t \gamma_\alpha(x,t) = 2iv\partial_x \gamma_\alpha(x,t) + i\frac{\tilde{t}_\alpha}{\sqrt{2}}\delta(x)[d(t) + d^\dagger(t)], \tag{A1}$$

$$i\partial_t d(t) = \varepsilon_d d - \sum_{\alpha=1,2} i\frac{\tilde{t}_\alpha}{2}\gamma_\alpha(0,t), \tag{A2}$$

$$i\partial_t d^\dagger(t) = -\varepsilon_d d^\dagger - \sum_{\alpha=1,2} i\frac{\tilde{t}_\alpha}{\sqrt{2}}\gamma_\alpha(0,t). \tag{A3}$$

After a Fourier transformation similar to Eqs. (5) and (6), we arrive at

$$\varepsilon\gamma_\alpha(x,\varepsilon) = 2iv\partial_x \gamma_\alpha(x,\varepsilon) + i\frac{\tilde{t}_\alpha}{\sqrt{2}}\delta(x)\gamma_0(\varepsilon), \tag{A4}$$

$$\varepsilon d(\varepsilon) = \varepsilon_d d(\varepsilon) - \sum_{\alpha=1,2} i\frac{\tilde{t}_\alpha}{\sqrt{2}}\gamma_\alpha(0,\varepsilon), \tag{A5}$$

$$\varepsilon d^\dagger(\varepsilon) = \varepsilon_d d^\dagger(\varepsilon) - \sum_{\alpha=1,2} i\frac{\tilde{t}_\alpha}{\sqrt{2}}\gamma_\alpha(0,\varepsilon). \tag{A6}$$

Integrating both sides of Eq. (A4) from 0^- to 0^+, we obtain

$$2iv[\gamma_\alpha(0^+) - \gamma_\alpha(0^-)] + i\frac{\tilde{t}_\alpha}{\sqrt{2}}(d + d^\dagger) = 0. \tag{A7}$$

Following the same procedure in the derivation of Eqs. (10), (11), and (12), the scattering matrix S_Q for the QD coupling case can be found,

$$S_Q = \frac{1}{\widetilde{A}}\begin{pmatrix} \widetilde{B} + \tilde{t}_2^2 - \tilde{t}_1^2 & -2\tilde{t}_1\tilde{t}_2 \\ -2\tilde{t}_1\tilde{t}_2 & \widetilde{B} + \tilde{t}_1^2 - \tilde{t}_2^2 \end{pmatrix}, \tag{A8}$$

where $\widetilde{B} = 4iv(\varepsilon^2 - \varepsilon_d^2)/\varepsilon$ and $\widetilde{A} = \widetilde{B} + \tilde{t}_1^2 + \tilde{t}_2^2$.

APPPENDIX B: TRANSMISSION COEFFICIENTS IN THE PROPOSED DEVICES

1. Device for the observation of the braidinglike operation

First, we consider the device that allows observing the braidinglike operation on chiral Majorana fermions based on TSC/QAHI junctions in Fig. 3(a). In the transport process of the four chiral Majorana fermions γ_i $(i = 1, 2, 3, 4)$, γ_1 and γ_4 are transported directly into lead 3 and lead 4 while γ_2 and γ_3 are scattered by the QD. For simplicity, denoting the incoming chiral Majorana fermions by γ_2 and γ_3 and outgoing scattering states by γ_2' and γ_3', respectively, the scattering matrix S_Q can be written as

$$\begin{pmatrix} \gamma_2' \\ \gamma_3' \end{pmatrix} = S_Q \begin{pmatrix} \gamma_2 \\ \gamma_3 \end{pmatrix}, \tag{B1}$$

where S_Q is given by Eqs. (15) and (A8). We define four operators as

$$a_1 = (\gamma_1 + i\gamma_2)/\sqrt{2}, \tag{B2}$$

$$a_2 = (\gamma_3 + i\gamma_4)/\sqrt{2}, \tag{B3}$$

$$b_3 = (\gamma_1 + i\gamma_2')/\sqrt{2}, \tag{B4}$$

$$b_4 = (\gamma_3' + i\gamma_4)/\sqrt{2}, \tag{B5}$$

which represent the incoming electron modes (a_1 from lead 1 and a_2 from lead 2) and outgoing electron modes (b_3 to lead 3 and b_4 to lead 4). By using Eq. (B1), we can obtain

$$b_3 = [(1+S_{Q,11})a_1+(1-S_{Q,11})a_1^\dagger + iS_{Q,12}a_2 + iS_{Q,12}a_2^\dagger]/2, \tag{B6}$$

$$b_3^\dagger = [(1-S_{Q,11}^*)a_1+(1+S_{Q,11}^*)a_1^\dagger - iS_{Q,12}^*a_2 - iS_{Q,12}^*a_2^\dagger]/2, \tag{B7}$$

$$b_4 = [-iS_{Q,21}a_1 + iS_{Q,21}a_1^\dagger + (1+S_{Q,22})a_2 + (-1+S_{Q,22})a_2^\dagger]/2, \tag{B8}$$

$$b_4^\dagger = [-iS_{Q,21}^*a_1 + iS_{Q,21}^*a_1^\dagger + (-1+S_{Q,22}^*)a_2 + (1+S_{Q,22}^*)a_2^\dagger]/2. \tag{B9}$$

These equations can be rewritten into a compact form as

$$\begin{pmatrix} b_3 \\ b_3^\dagger \\ b_4 \\ b_4^\dagger \end{pmatrix} = \overrightarrow{S} \begin{pmatrix} a_1 \\ a_1^\dagger \\ a_2 \\ a_2^\dagger \end{pmatrix}, \tag{B10}$$

with

$$\overrightarrow{S} = \frac{1}{2}\begin{pmatrix} 1+S_{Q,11} & 1-S_{Q,11} & iS_{Q,12} & iS_{Q,12} \\ 1-S_{Q,11}^* & 1+S_{Q,11}^* & -iS_{Q,12}^* & -iS_{Q,12}^* \\ -iS_{Q,21} & iS_{Q,21} & 1+S_{Q,22} & -1+S_{Q,22} \\ -iS_{Q,21}^* & iS_{Q,21}^* & -1+S_{Q,22}^* & 1+S_{Q,22}^* \end{pmatrix}. \tag{B11}$$

Then the transport coefficients for normal tunneling and Andreev reflection from lead 1 to lead 3 and lead 4 can be obtained by

$$T_{31}(\varepsilon) = |\overrightarrow{S}_{11}|^2 = |1+S_{Q,11}|^2/4, \tag{B12}$$

$$T_{31}^A(\varepsilon) = |\overrightarrow{S}_{21}|^2 = |1-S_{Q,11}^*|^2/4, \tag{B13}$$

$$T_{41}(\varepsilon) = |\overrightarrow{S}_{31}|^2 = |iS_{Q,21}|^2/4, \tag{B14}$$

$$T_{41}^A(\varepsilon) = |\overrightarrow{S}_{41}|^2 = |iS_{Q,21}^*|^2/4. \tag{B15}$$

Considering the finite temperature $\mathcal{T}$, the effective transmission coefficients can be derived:

$$T_{31(41)} = \int_{-\infty}^{+\infty} T_{31(41)}(\varepsilon)\left(-\frac{\partial f}{\partial \varepsilon}\right)d\varepsilon, \tag{B16}$$

$$T_{31(41)}^A = \int_{-\infty}^{+\infty} T_{31(41)}^A(\varepsilon)\left(-\frac{\partial f}{\partial \varepsilon}\right)d\varepsilon, \tag{B17}$$

where $f(\varepsilon) = [\exp(\varepsilon/k_B\mathcal{T})+1]^{-1}$ is the Fermi distribution function.

2. Device for the observation of non-Abelian character

We now calculate the transport properties of the four chiral Majorana fermions after sequential exchanges in Fig. 4. If the final state depends on the operation order as well as the measurement of terminal conductance, this means that the braidinglike operation on chiral Majorana fermions has non-Abelian character. First, we consider the joint operations with two exchanges, $\sigma_2\sigma_1$ and $\sigma_1\sigma_2$. $\sigma_2\sigma_1$ will transform the four chiral Majorana fermions according to $(\gamma_1, \gamma_2, \gamma_3, \gamma_4) \rightarrow (-\gamma_2, -\gamma_3, \gamma_1, \gamma_4)$. After the braidinglike operations, the outgoing electron modes (b_3 to lead 3 and b_4 to lead 4) now become

$$b_3 = (-\gamma_2 - i\gamma_3)/\sqrt{2} = (ia_1 - ia_1^\dagger - ia_2 - ia_2^\dagger)/2,$$
$$b_3^\dagger = (-\gamma_2 + i\gamma_3)/\sqrt{2} = (ia_1 - ia_1^\dagger + ia_2 + ia_2^\dagger)/2,$$
$$b_4 = (\gamma_1 + i\gamma_4)/\sqrt{2} = (a_1 + a_1^\dagger + a_2 - a_2^\dagger)/2,$$
$$b_4^\dagger = (\gamma_1 - i\gamma_4)/\sqrt{2} = (a_1 + a_1^\dagger - a_2 + a_2^\dagger)/2,$$

where we have used $\gamma_1 = \frac{1}{\sqrt{2}}(a_1 + a_1^\dagger)$, $\gamma_2 = \frac{1}{i\sqrt{2}}(a_1 - a_1^\dagger)$, $\gamma_3 = \frac{1}{\sqrt{2}}(a_2 + a_2^\dagger)$, $\gamma_4 = \frac{1}{i\sqrt{2}}(a_2 - a_2^\dagger)$. Now, the scattering matrix $\overrightarrow{S}$ relating the incoming modes $a_{1,2}, a_{1,2}^\dagger$ and $b_{3,4}, b_{3,4}^\dagger$ becomes

$$\overrightarrow{S} = \frac{1}{2}\begin{pmatrix} i & -i & -i & -i \\ i & -i & i & i \\ 1 & 1 & 1 & -1 \\ 1 & 1 & -1 & 1 \end{pmatrix}, \tag{B18}$$

which gives $T_{31} = T_{41} = T_{31}^A = T_{41}^A = 1/4$ and $T_{32} = T_{42} = T_{32}^A = T_{42}^A = 1/4$. By using these normal tunneling and Andreev reflection coefficients, the conductances can be obtained from Eqs. (17)–(21), and the results are $G_3 = G_4 = \frac{e^2}{2h}$. Similarly, the scattering matrix for the joint operation $\sigma_1\sigma_2$ can be obtained following the same procedure as

$$\overrightarrow{S} = \frac{1}{2}\begin{pmatrix} i & i & 1 & 1 \\ -i & -i & 1 & 1 \\ -i & i & 1 & -1 \\ -i & i & -1 & 1 \end{pmatrix}; \tag{B19}$$

thus, it gives the same terminal conductance $G_3 = G_4 = \frac{e^2}{2h}$ as $\sigma_2\sigma_1$ even though the final states are different.

Next, we turn to the joint operators $\sigma_2\sigma_1\sigma_2$ and $\sigma_2\sigma_2\sigma_1$. After the transformation by $\sigma_2\sigma_1\sigma_2$, $(\gamma_1, \gamma_2, \gamma_3, \gamma_4)$ becomes

$(\gamma_3, -\gamma_2, \gamma_1, \gamma_4)$, and the resulting scattering matrix is

$$\overrightarrow{S} = \frac{1}{2}\begin{pmatrix} -1 & 1 & 1 & 1 \\ 1 & -1 & 1 & 1 \\ 1 & 1 & 1 & -1 \\ 1 & 1 & -1 & 1 \end{pmatrix}. \tag{B20}$$

We obtain $T_{31} = T_{41} = T_{31}^A = T_{41}^A = 1/4$ and $T_{32} = T_{42} = T_{32}^A = T_{42}^A = 1/4$, and $G_3 = G_4 = \frac{e^2}{2h}$ again. However, the joint operator $\sigma_2\sigma_2\sigma_1$ transforms the chiral Majorana fermions γ_i according to $(\gamma_1, \gamma_2, \gamma_3, \gamma_4) \to (-\gamma_2, -\gamma_1, -\gamma_3, \gamma_4)$. The related scattering matrix now becomes

$$\overrightarrow{S} = \begin{pmatrix} 0 & -i & 0 & 0 \\ i & 0 & 0 & 0 \\ 0 & 0 & 0 & -1 \\ 0 & 0 & 1 & 0 \end{pmatrix}, \tag{B21}$$

which gives $T_{31}^A = T_{42}^A = 1$ and $T_{31} = T_{41} = T_{41}^A = T_{32} = T_{42} = T_{42}^A = 0$. The corresponding terminal conductances are $G_4 = \frac{e^2}{h}$ and $G_3 = 0$.

[1] J. Alicea, Rep. Prog. Phys. **75**, 076501 (2012).
[2] C. W. J. Beenakker, Annu. Rev. Condens. Matter Phys. **4**, 113 (2013).
[3] S. Das Sarma, M. Freedman, and C. Nayak, npj Quantum Inf. **1**, 15001 (2015).
[4] N. Read and D. Green, Phys. Rev. B **61**, 10267 (2000).
[5] D. A. Ivanov, Phys. Rev. Lett. **86**, 268 (2001).
[6] A. Kitaev, Ann. Phys. (NY) **303**, 2 (2003).
[7] M. H. Freedman, M. Larsen, and Z. Wang, Commun. Math. Phys. **227**, 605 (2002).
[8] S. Das Sarma, M. Freedman, and C. Nayak, Phys. Rev. Lett. **94**, 166802 (2005).
[9] C. Nayak, S. H. Simon, A. Stern, M. Freedman, and S. Das Sarma, Rev. Mod. Phys. **80**, 1083 (2008).
[10] J. Alicea, Y. Oreg, G. Refael, F. von Oppen, and M. P. A. Fisher, Nat. Phys. **7**, 412 (2011).
[11] G. Moore and N. Read, Nucl. Phys. B **360**, 362 (1991).
[12] I. P. Radu, J. B. Miller, C. M. Marcus, M. A. Kastner, L. N. Pfeiffer, and K. W. West, Science **320**, 899 (2008).
[13] M. Dolev, M. Heiblum, V. Umansky, A. Stern, and D. Mahalu, Nature (London) **452**, 829 (2008).
[14] G. E. Volovik, JETP Lett. **70**, 609 (1999).
[15] L. Fu and C. L. Kane, Phys. Rev. Lett. **100**, 096407 (2008).
[16] H.-H. Sun, K.-W. Zhang, L.-H. Hu, C. Li, G.-Y. Wang, H.-Y. Ma, Z.-A. Xu, C.-L. Gao, D.-D. Guan, Y.-Y. Li, C. Liu, D. Qian, Y. Zhou, L. Fu, S.-C. Li, F.-C. Zhang, and J.-F. Jia, Phys. Rev. Lett. **116**, 257003 (2016).
[17] A. Y. Kitaev, Phys.-Usp. **44**, 131 (2001).
[18] R. M. Lutchyn, J. D. Sau, and S. Das Sarma, Phys. Rev. Lett. **105**, 077001 (2010).
[19] Y. Oreg, G. Refael, and F. von Oppen, Phys. Rev. Lett. **105**, 177002 (2010).
[20] V. Mourik, K. Zuo, S. M. Frolov, S. R. Plissard, E. P. A. M. Bakkers, and L. P. Kouwenhoven, Science **336**, 1003 (2012).
[21] A. Das, Y. Ronen, Y. Most, Y. Oreg, M. Heiblum, and H. Shtrikman, Nat. Phys. **8**, 887 (2012).
[22] M. T. Deng, S. Vaitiekėnas, E. B. Hansen, J. Danon, M. Leijnse, K. Flensberg, J. Nygård, P. Krogstrup, and C. M. Marcus, Science **354**, 1557 (2016).
[23] H. Zhang, C. X. Liu, S. Gazibegovic, D. Xu, J. A. Logan, G. Wang, N. van Loo, J. D. S. Bommer, M. W. A. de Moor, D. Car, R. L. M. Op het Veld, P. J. van Veldhoven, S. Koelling, M. A. Verheijen, M. Pendharkar, D. J. Pennachio, B. Shojaei, J. S. Lee, C. J. Palmstrøm, E. P. A. M. Bakkers, S. Das Sarma, and L. P. Kouwenhoven, Nature (London) **556**, 74 (2018).
[24] T. Hyart, B. van Heck, I. C. Fulga, M. Burrello, A. R. Akhmerov, and C. W. J. Beenakker, Phys. Rev. B **88**, 035121 (2013).
[25] S. Plugge, A. Rasmussen, R. Egger, and K. Flensberg, New J. Phys. **19**, 012001 (2016).
[26] T. Karzig, C. Knapp, R. M. Lutchyn, P. Bonderson, M. B. Hastings, C. Nayak, J. Alicea, K. Flensberg, S. Plugge, Y. Oreg, C. M. Marcus, and M. H. Freedman, Phys. Rev. B **95**, 235305 (2017).
[27] C. Malciu, L. Mazza, and C. Mora, Phys. Rev. B **98**, 165426 (2018).
[28] A. P. Mackenzie and Y. Maeno, Rev. Mod. Phys. **75**, 657 (2003).
[29] X.-L. Qi, T. L. Hughes, and S.-C. Zhang, Phys. Rev. B **82**, 184516 (2010).
[30] J. D. Sau, R. M. Lutchyn, S. Tewari, and S. Das Sarma, Phys. Rev. Lett. **104**, 040502 (2010).
[31] G. Strübi, W. Belzig, M.-S. Choi, and C. Bruder, Phys. Rev. Lett. **107**, 136403 (2011).
[32] R. Žitko and P. Simon, Phys. Rev. B **84**, 195310 (2011).
[33] J. Wang, Q. Zhou, B. Lian, and S.-C. Zhang, Phys. Rev. B **92**, 064520 (2015).
[34] Y.-F. Zhou, Z. Hou, Y.-T. Zhang, and Q.-F. Sun, Phys. Rev. B **97**, 115452 (2018).
[35] O. Viyuela, L. Fu, and M. A. Martin-Delgado, Phys. Rev. Lett. **120**, 017001 (2018).
[36] Y.-H. Li, J. Liu, H. Liu, H. Jiang, Q.-F. Sun, and X. C. Xie, Phys. Rev. B **98**, 045141 (2018).
[37] Y.-F. Zhou, Z. Hou, P. Lv, X. C. Xie, and Q.-F. Sun, Sci. China: Phys. Mech. Astron. **61**, 127811 (2018).
[38] C.-Z. Chang, J. Zhang, X. Feng, J. Shen, Z. Zhang, M. Guo, K. Li, Y. Ou, P. Wei, L.-L. Wang, Z.-Q. Ji, Y. Feng, S. Ji, X. Chen, J. Jia, X. Dai, Z. Fang, S.-C. Zhang, K. He, Y. Wang, L. Lu, X.-C. Ma, and Q.-K. Xue, Science **340**, 167 (2013).
[39] A. Kandala, A. Richardella, S. Kempinger, C.-X. Liu, and N. Samarth, Nat. Commun. **6**, 7434 (2015).
[40] Q. L. He, L. Pan, A. L. Stern, E. C. Burks, X. Che, G. Yin, J. Wang, B. Lian, Q. Zhou, E. S. Choi, K. Murata, X. Kou, Z. Chen, T. Nie, Q. Shao, Y. Fan, S.-C. Zhang, K. Liu, J. Xia, and K. L. Wang, Science **357**, 294 (2017).
[41] B. Lian, X.-Q. Sun, A. Vaezi, X.-L. Qi, and S.-C. Zhang, Proc. Natl. Acad. Sci. USA **115**, 10938 (2018).
[42] C. W. J. Beenakker, P. Baireuther, Y. Herasymenko, I. Adagideli, L. Wang, and A. R. Akhmerov, Phys. Rev. Lett. **122**, 146803 (2019).
[43] C. W. J. Beenakker, Phys. Rev. B **44**, 1646 (1991).

[44] Q.-F. Sun and T.-H. Lin, J. Phys.: Condens. Matter **9**, 4875 (1997).
[45] J. R. Petta, A. C. Johnson, J. M. Taylor, E. A. Laird, A. Yacoby, M. D. Lukin, C. M. Marcus, M. P. Hanson, and A. C. Gossard, Science **309**, 2180 (2005).
[46] F. H. L. Koppens, C. Buizert, K. J. Tielrooij, I. T. Vink, K. C. Nowack, T. Meunier, L. P. Kouwenhoven, and L. M. K. Vandersypen, Nature (London) **442**, 766 (2006).
[47] F. A. Zwanenburg, A. S. Dzurak, A. Morello, M. Y. Simmons, L. C. L. Hollenberg, G. Klimeck, S. Rogge, S. N. Coppersmith, and M. A. Eriksson, Rev. Mod. Phys. **85**, 961 (2013).
[48] H. S. Røising and S. H. Simon, Phys. Rev. B **97**, 115424 (2018).
[49] K. T. Law, P. A. Lee, and T. K. Ng, Phys. Rev. Lett. **103**, 237001 (2009).
[50] Y.-T. Zhang, Z. Hou, X. C. Xie, and Q.-F. Sun, Phys. Rev. B **95**, 245433 (2017).
[51] Q.-F. Sun and X. C. Xie, J. Phys.: Condens. Matter **21**, 344204 (2009).
[52] S.-G. Cheng, Y. Xing, J. Wang, and Q.-F. Sun, Phys. Rev. Lett. **103**, 167003 (2009).
[53] S. Datta, *Electronic Transport in Mesoscopic System* (Cambridge University Press, Cambridge, 1995).
[54] T. Karzig, G. Refael, and F. von Oppen, Phys. Rev. X **3**, 041017 (2013).
[55] M. S. Scheurer and A. Shnirman, Phys. Rev. B **88**, 064515 (2013).
[56] D. J. Thouless, Phys. Rev. Lett. **39**, 1167 (1977).
[57] T. Martin and S. Feng, Phys. Rev. Lett. **64**, 1971 (1990).
[58] S. Koch, R. J. Haug, K. V. Klitzing, and K. Ploog, Phys. Rev. Lett. **67**, 883 (1991).
[59] L. Fu and C. L. Kane, Phys. Rev. Lett. **102**, 216403 (2009).